Received: 13 June 2024 | Revised: 27 July 2024 | Accepted: 31 July 2024

DOI: 10.1002/mrm.30257

Magnetic Resonance in Medicine

TECHNICAL NOTE

On the impact of B0 shimming algorithms on single-voxel MR spectroscopy

Behrouz Vejdani Afkham[1] | **Eva Alonso-Ortiz**[1,2]

[1]NeuroPoly Lab, Institute of Biomedical Engineering, Polytechnique Montréal, Montréal, Quebec Canada

[2]Centre de recherche du CHU Sainte-Justine, Montréal, Quebec Canada

Correspondence
Eva Alonso-Ortiz, École Polytechnique, Department of Electrical Engineering, 2900 Edouard-Montpetit Montreal, QC, H3T 1J4 Canada.
Email: eva.alonso-ortiz@polymtl.ca

Funding information
Natural Sciences and Engineering Research Council of Canada; Institut TransMedTech; Polytechnique Montréal

Abstract

Purpose: To assess the impact of different B0 shimming algorithms on MRS.

Methods: B0 field maps and single-voxel MR spectroscopy were acquired in the prefrontal cortex of five volunteers at 3 T using five different B0 shimming approaches. B0 shimming was achieved using Siemens' proprietary shim algorithm, in addition to the Pseudo-Inverse (PI), Quadratic Programming (QuadProg), Least Squares (LSq), and Gradient optimization (Grad) algorithms. The standard deviation of the shimmed B0 field, as well as the SNR and FWHM of the measured metabolites, was used to evaluate the performance of each B0 shimming algorithm.

Results: Compared to Siemens's shim, significant reductions ($p < 0.01$) in the standard deviation of the B0 field distribution within the MRS voxel were observed for the PI, QuadProg, and Grad algorithms (3.8 Hz, 7.3 Hz, and 3.9 Hz respectively, compared to 11.5 Hz for Siemens), but not for the LSq (12.9 Hz) algorithm. Moreover, significantly increased SNR and reduced FWHM for the *N*-acetylaspartate metabolite were consistent with the improvement in B0 homogeneity for the aforementioned shimming algorithms.

Conclusion: Here, we demonstrate that the choice of B0 shimming algorithm can have a significant impact on the quality of MR spectra and that significant improvements in spectrum quality could be achieved by using alternatives to the default vendor approach.

KEYWORDS

B0 shimming, magnetic resonance spectroscopy, metabolites, neuroimaging

1 | INTRODUCTION

MR spectroscopy (MRS) is a powerful MRI technique that is used to measure brain metabolites, such as *N*-acetylaspartate (NAA), creatine (Cr), choline (Cho), etc. Although well-established for assessing brain pathologies, the high sensitivity of MRS to inhomogeneities in the main magnetic field (B0) presents a challenge for obtaining high-quality spectra. B0 shimming is the process of homogenizing the B0 field by creating compensatory magnetic fields, usually by using spherical harmonic (SH) shim coils.[1] Poor B0 shimming negatively affects MRS by

broadening the metabolites' linewidths, leading to erroneous fitting of metabolite concentrations due to overlapping peaks.[2]

The spectral linewidth or FWHM can be expressed as a combination of intrinsic spin–spin ($T2$) relaxation time plus microscopic and macroscopic B0 offsets (ΔB0)[3]:

$$\mathrm{FWHM} = \left(\frac{1}{\pi \cdot T2}\right) + \Delta B0_{\mathrm{micro}} + \Delta B0_{\mathrm{macro}} \qquad (1)$$

$\Delta B0_{\mathrm{macro}}$ is a key contributor to linewidth broadening that can be mitigated through B0 shimming. However, microscopic offsets arising from tissue heterogeneity at the micro-scale remain uncorrectable. Both $\Delta B0_{\mathrm{micro}}$ and $\Delta B0_{\mathrm{macro}}$ increase the FWHM of spectral peaks through spin dephasing. Thus, suboptimal B0 shimming results in reduced SNR and increased FWHM of spectral peaks.

In addition to the widening of linewidths, inadequate B0 shimming also leads to ineffective water suppression, as the latter relies on the calibrated central frequency.[4] Another important issue arising from an inhomogeneous B0 field is the mislocalization of the MRS voxel position, given that spatial encoding is based on the assumption of linear field distributions across the imaging volume.[2] These issues are particularly critical in the frontal lobe, where strong B0 variations occur due to the difference in magnetic susceptibility between air in nasal and sphenoid sinuses and adjacent brain tissues.[5] The prefrontal cortex (PFC), a region of neurological significance frequently targeted in single-voxel MRS of neurodegenerative disease,[6] highlights the importance of proper B0 shimming for successful MRS. While some of the B0 inhomogeneity-induced artifacts can be eliminated in MRI using various post-processing methods,[7,8] these are not viable for MRS, underscoring the importance of effective B0 shimming.[2] B0 shimming is achieved by acquiring a B0 map that will subsequently be decomposed into a set of SH shim functions. The scanner's SH shim coils are then used to generate spatially varying fields of opposite polarity to cancel the measured inhomogeneity.[9] The decomposition of the measured B0 map into a linear combination of SH shims is carried out by an optimization solver, the efficacy of which varies depending on the optimization algorithm and the nature of the employed objective function.

Various studies have explored B0 shimming in the context of MRS. Some work has focused on B0 mapping and its impact on shimming,[10-12] while others have focused on assessing different shimming approaches.[13,14] Typically, a volume-wise B0 map is acquired for subsequent B0 shimming. However, this process can be time consuming. Alternative, projection-based or pencil beam B0 measurements such as FASTMAP,[15,16] FASTERMAP,[17] and FASTESTMAP[18] can be used, where multiple one-dimensional projections of the B0 field at different angles are measured. While the latter saves time, it might not accurately reflect the true inhomogeneity since it relies on a limited number of projections to approximate the field. A recent study confirmed this by comparing the shimming outcome achieved with FASTESTMAP to that of B0 mapping.[13] In a study by Zhong et al.[12] they compared FASTESTMAP to 3D gradient echo (GRE) field mapping and an "advanced" shim mode on a 3 T Siemens scanner. The "advanced" shim mode uses a DESS (Double-Echo Steady State) sequence with reversed gradient polarities for eddy-current correction. Zhong et al. observed comparable performance between the first two methods, both of which outperformed the advanced mode. They demonstrated that shimming with both FASTESTMAP and 3D GRE reduced the FWHM of the water peak compared to the advanced mode. Liao et al. also compared B0 homogeneity and the FWHM of water after shimming at 3 T and 7 T[10] using the "brain" and "advanced" shim modes (which represent different B0 mapping acquisition protocols) for single voxel MRS on a Siemens scanner. They found that the "brain" shim mode outperforms the "advanced" mode at 3 T, whereas the "advanced" mode was superior at 7 T. When comparing the Siemens-provided "advanced" shim mode to FASTESTMAP B0 shimming, Deelchand et al.[11] reported a significant improvement in the MRS spectral linewidth of water: 10.5 Hz with the former vs 6.1 Hz with the latter. However, they attributed this improvement to the higher resolution that was used with FASTESTMAP compared to that which was used with the "advanced" mode (1.2 mm vs. 8 mm, respectively). Other works have focused on assessing the impact of including higher-order SH shim coils for B0 shimming in MRS. To this effect, Chang et al.[20] showed that at 9.4 T, second-order SH shims were sufficient when shimming a single MRS voxel located in the frontal lobe, and that including higher-order terms did not significantly alter the water linewidth. On the other hand, a 2023 study by Pan et al.[13] showed that 7 T single-voxel MRS in the PFC does benefit from shimming using up to 4th-order SH shims in conjunction with map-based B0 shimming.

Beyond the effects of different B0 mapping methods on B0 shimming, or up to which order SH shims should be included, lie additional questions. To assess the efficacy of different optimization algorithms on B0 shimming, Nassirpour et al.[14] compared 10 different algorithms, including a newly introduced regularized method; constrained truncated singular value decomposition inversion (ConsTru), for shimming a $2 \times 2 \times 2\,\mathrm{cm}^3$ voxel in the frontal cortex at 7 T. They found that ConsTru led to the best shim quality and proceeded to acquire MRS data in the frontal cortex at 9.4 T using both ConsTru and Siemens' proprietary algorithm for B0 shimming. They found that

measured water FWHM values were considerably lower when shimming using up to second-order SH shims with ConsTru versus Siemens' algorithm. Nassirpour et al. recommended using a regularized optimization algorithm for B0 shimming over generic solvers. Nevertheless, it remains unclear whether a regularized algorithm is in fact necessary at lower field strengths, such as 3 T, given the inherently lower B0 inhomogeneity. Here, our goal was to compare both shimmed B0 fields and single-voxel MRS spectra in the PFC when using various B0 shim optimization algorithms, including Siemens' default algorithm, on a 3 T scanner.

2 | METHODS

2.1 | Data acquisition

Five healthy volunteers were recruited for this study and imaging was performed on a 3 T Siemens Prisma-Fit MRI scanner using a 64-channel head and neck coil. Informed consent was given prior to scanning (study approved by the Comité d'éthique de la recherche du Regroupement Neuroimagerie Québec).

The imaging session began with an anatomical (MP2RAGE) scan (TR = 3000 ms, TE = 3.39 ms, 1.5 mm slice thickness, in-plane resolution of 1.1 x 1.1 mm^2, acquisition time of 3 m 44 s, and GRAPPA factor of 3). The remainder of the scanning session can be broken down into two steps:

2.1.1 | Step 1: MRS using Siemens' shim optimization algorithm

(a) A Point REsolved SpectroScopy (PRESS) sequence was used to position a 20 x 20 x 20 mm^3 MRS voxel in the PFC. A B0 shim box was centered on the MRS voxel and set to cover ~26 x 26 x 26 mm^3. (b) The initial B0 shim coefficients were set to the system's "Tune up" values and a central frequency (f0) adjustment was performed. (c) Next, a whole-brain B0 map was acquired using the "brain" B0 mapping protocol (3D dual-echo GRE, TR = 9 ms, TE1/TE2: 2.39/7.17 ms, 64 x 54 matrix, 26 slices, FA = 15°, 4.4 mm^3 isotropic resolution, total acquisition time = 11 s), which is pre-defined by Siemens and can be selected among a list of B0 mapping protocols within Siemens' B0 shimming tool. (d) Siemens' proprietary shim algorithm was run using the acquired whole-brain B0 map and the B0 shim box. (e) The resulting shim coefficients were applied and f0 was re-adjusted. (f) After B0 shimming, the PRESS sequence (TR = 2000 ms, TE = 135 ms, BW = 1200 Hz, voxel size: 20 x 20 x 20 mm^3, total acquisition time = 4 m 26 s) was acquired. (g) This was followed by a 3D dual-echo GRE sequence with a protocol that was set to match that of Siemens' "brain" B0 mapping sequence. This GRE sequence was acquired with the same B0 shim coefficients and f0 as the PRESS sequence to measure the B0 field after shimming with Siemens' approach. The duration for step 1 was ~6 m with an interval of 1 m 30 sec between B0 mapping and the start of the MRS acquisition.

2.1.2 | Step 2: MRS using alternative shim optimization algorithms

(a) A new MRS voxel and B0 shim box was positioned in the same location as Step 1a. (b) The B0 shim coefficients were set to the system's "Tune up" values and the f0 obtained in Step 1b was applied. (c) A new 3D dual-echo GRE scan with identical parameters to that of Step 1c was acquired. (d) The anatomical scan, MRS data from Step 1f, and newly acquired GRE data were transferred via ethernet to an external laptop running the Shimming-Toolbox.[21] The anatomical scan was used to generate a brain mask and the dual-echo GRE data were processed using the aforementioned brain mask, resulting in a whole-brain B0 map. The MRS voxel position was extracted from the MRS data so that the same 26 x 26 x 26 mm^3 B0 shim volume from step 2a could be defined on the B0 map. First- and second-order SH shim optimization within the B0 shim volume was performed. (e) Once the Shimming-Toolbox completed the shim optimization, the optimized shim coefficients were input into the scanner's system and a new f0 adjustment was performed. (f) A new MRS voxel was acquired using the same acquisition parameters listed in Step 1f. (g) Another 3D dual-echo GRE sequence with a protocol that was set to match that of Siemens' "brain" B0 mapping sequence was acquired with the same B0 shim coefficients and f0 as the PRESS sequence to measure the B0 field after shimming with an alternative shim optimization algorithm. The duration for step 2 was on average ~7 m 30 s with an interval of 2 m 30 s between B0 mapping and the start of the MRS acquisition.

Step 2 was repeated 4 times, using each of the following shim optimization algorithms:

Unconstrained Pseudo-Inverse (PI): The coil shim coefficients (or weights), C (an m x 1 vector, where m is the number of shim terms), are obtained by inverting the scanner's coil profiles, M (an n x m matrix):

$$C = M^{\dagger} B0 \tag{2}$$

where $B0$ is an n x 1 vector representing a measured B0 map of n total voxels and $M^{\dagger}$ is the PI of M. Unlike iterative

optimization methods, this approach does not require an initial guess and always yields the best achievable solution. However, this algorithm does not consider the minimum and maximum currents that can be applied to the MRI system's shim coils (i.e., it is unconstrained).

Constrained Quadratic Programming (QuadProg): This algorithm is based on the study of Goldfarb and Idnani,[22] where the unconstrained solution of Eq. (3) is used as the starting point for the optimization. For this algorithm, the Python solver *quadprog* was used. The shim coefficients are obtained by minimizing:

$$\left(1/2\, C^T\, D\, C - d^T C \right) \tag{3}$$

where $d^T = B0^T M$, $D = M^T M$, and superscript T denotes transpose.

Constrained Least Squares (LSq): This algorithm uses the *SLSQP* method implemented in Python's SciPy library. Here, the Jacobian of the loss function is computed with respect to the variables and passed to the algorithm to avoid additional time for estimating it at each iteration. The shim coefficients are obtained by minimizing:

$$\| MC - B0 \|^2. \tag{4}$$

Bound-constraint gradient-based optimizer (Grad): The Grad algorithm[23] is a quasi-Newton method designed to solve a nonlinear problem with a large number of variables while also considering bounds on the variables.[24] The algorithm is based on the *L-BFGS-B* method from Python's SciPy library. We introduced a pseudo-Huber loss function to this algorithm, as it combines the desirable attributes of the absolute and quadratic loss function, rendering the Grad algorithm less sensitive to outliers and allowing it to converge faster.[25]

All constrained algorithms were subject to the minimum and maximum current constraints of the system's coils. The QuadProg and LSq also consider the absolute sum of currents over all channels. The average run times for each method were: 6.11 s, 5.25 s, 6.42 s, and 7.02 s for PI, QuadProg, LSq, and Grad algorithms, respectively. These run times are calculated from an average of 150 test runs on a system with a 2.2 GHz 6-Core Intel CPU and 16 GB of RAM. The acquired B0 maps, MRS data, and processing code have been made open-access and can be found on OSF and GitHub (URLs under Data Availability) (Figure 1).

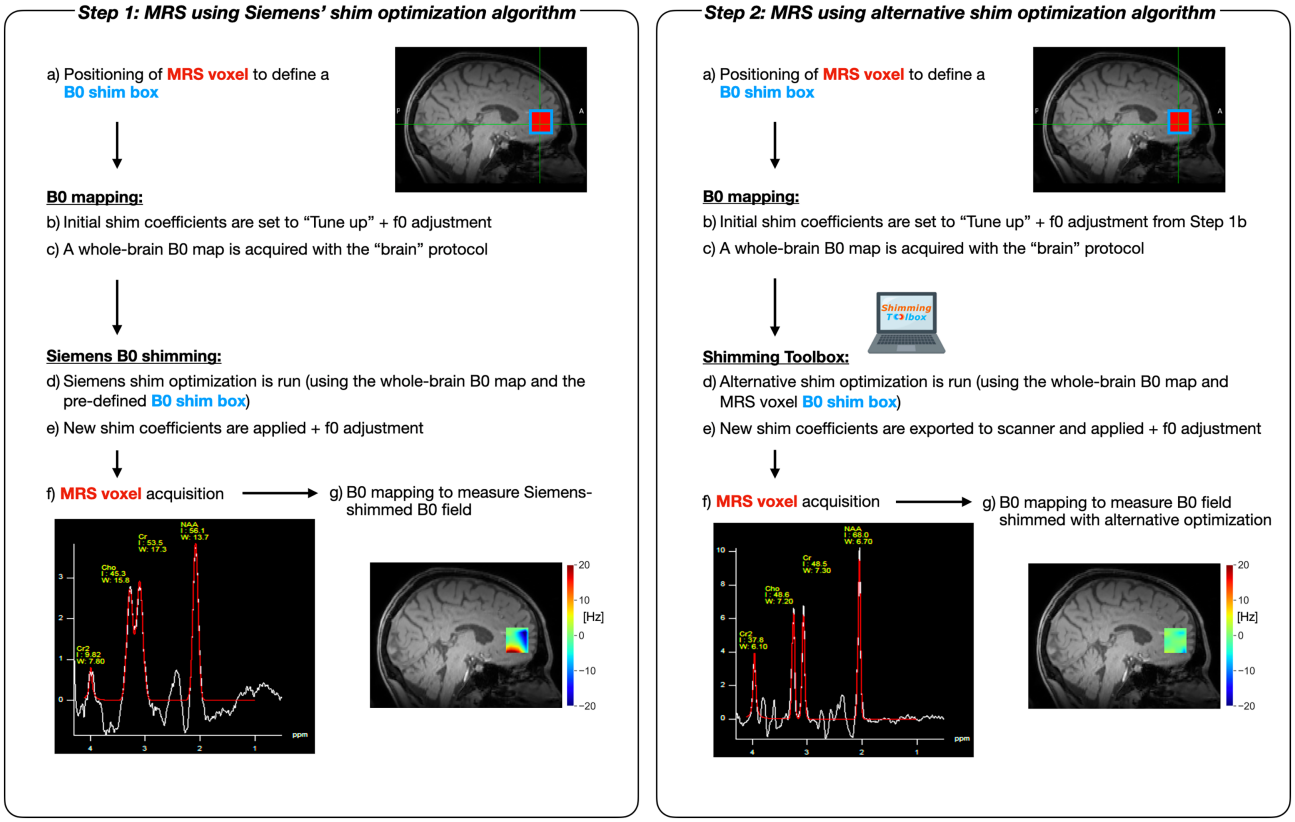

FIGURE 1 The data acquisition process for B0 shimming using Siemens' shim optimization algorithm (Step 1) vs. alternative shim optimization algorithms (Step 2), followed by MRS data acquisition. The spectra and the B0 map in Step 2 were obtained with the Grad algorithm.

2.2 | Post-processing and data analysis

The Shimming-Toolbox was used to generate a B0 map from the dual-echo GRE data from Steps 1g and 2g. A Kolmogorov–Smirnov test was applied to assess the normality of the distribution of B0 offsets within the MRS voxel volume for each algorithm. Upon establishing a non-normal distribution, the Levene test was employed to examine whether those distributions were significantly different. The significance level (p-value) was chosen to be below 0.01 and Bonferroni adjustments were applied to correct for multiple comparisons.

The analysis of the MRS data, including water peak removal and fitting of the spectra, was done using the FSL-MRS package.[26] The simulation of the basis set, which serves as the reference for fitting, was conducted using MRSCloud.[27]

The algorithms were ranked by comparing key metabolite characteristics, including FWHM and SNR, and Cramer-Rao lower bounds (CRLB) which is a measure of the fit uncertainty.[28]

3 | RESULTS

The individual-subjects' B0 offset distributions were normalized before and after shimming and subsequently grouped together. In Figure 2 we show the agglomerated distribution of B0 offsets within the acquired MRS voxel for each shimming algorithm. Compared to Siemens's shim, significant reductions in the standard deviation (SD) of the B0 distribution are apparent for the PI, Grad, and QuadProg methods (3.8 Hz, 3.9 Hz, and 7.3 Hz, respectively, compared to 11.5 Hz for Siemens). However, there

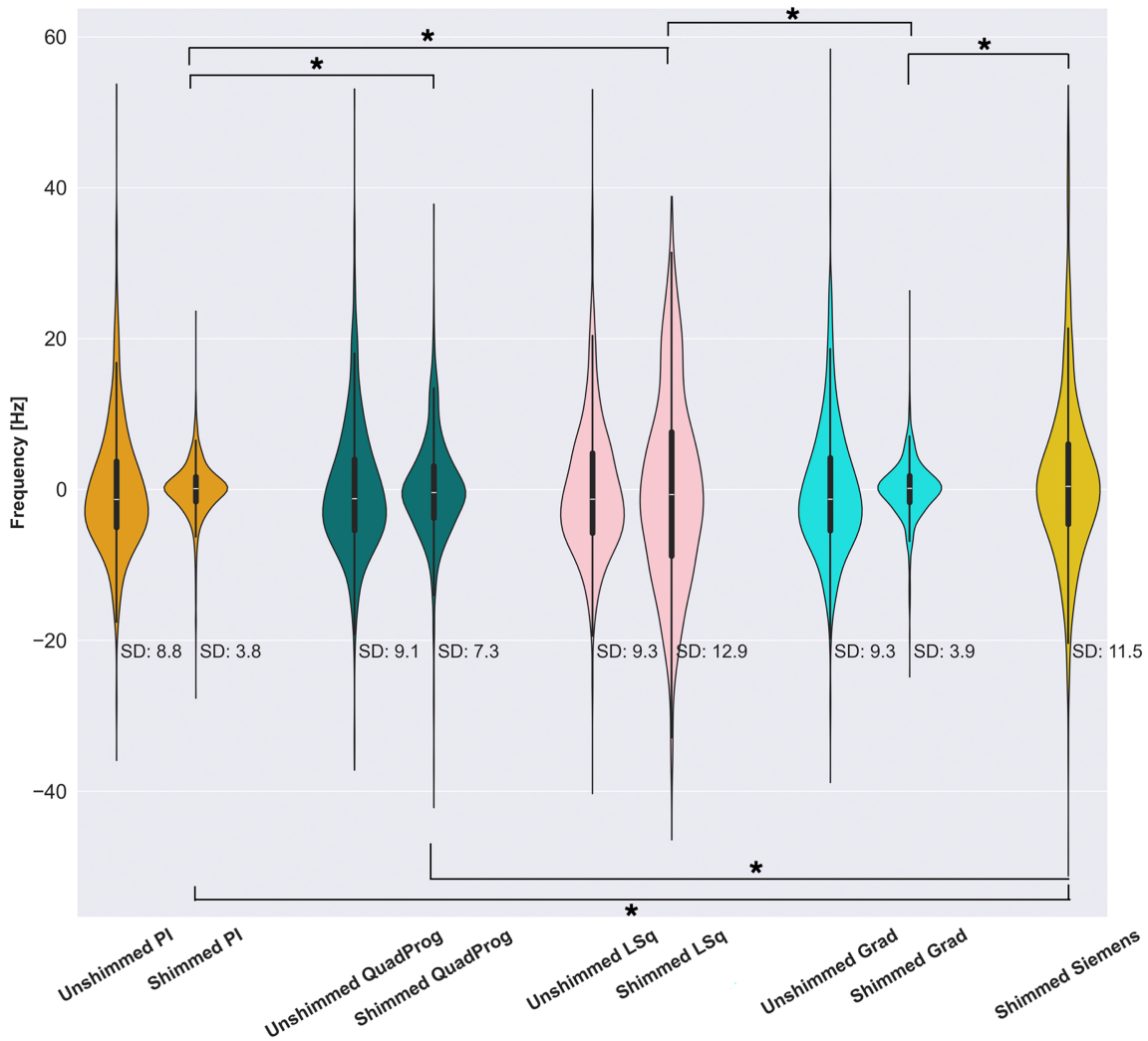

FIGURE 2 The distribution of B0 offsets (in the form of a violin plot) within the MRS voxel volume of all subjects obtained before and after shimming with each algorithm. The standard deviation (SD) is displayed next to each violin plot. Significantly different ($p < 0.01$) distributions are highlighted with an asterisk.

was no significant reduction in the within-MRS-voxel SD between the LSq algorithm and that of Siemens (12.9 Hz vs. 11.5 Hz).

The inter-subject variability for each algorithm was also assessed by computing the SD of the individual subject's SDs. This measure for the PI, QuadProg, LSq, Grad, and Siemens algorithms was 0.9 Hz, 2.3 Hz, 2.9 Hz, 1.1 Hz, and 3.3 Hz, respectively.

For the comparison of spectra quality (FWHM, SNR, and CRLB) across the different shimming algorithms, we focused on the NAA (2 ppm) metabolite, which is commonly used in clinical diagnosis and for reporting the FWHM and SNR.[29] Figure 3 displays the fitted spectra for a single representative subject with each shimming algorithm. Observing this figure, it is evident that the LSq algorithm exhibits significant baseline distortion and overlapping of Cr (3 ppm) and Cho (3.2 ppm) peaks, coinciding with the increased SD of the B0 map following shimming with this optimizer, compared to no shimming. Conversely, both the Grad and PI methods demonstrated a comparable level of superior performance (sharp peaks and flat baseline) compared to the other algorithms.

In Figure 4, we show scatter plots of the FWHM, SNR, and CRLB of NAA obtained with each shim algorithm

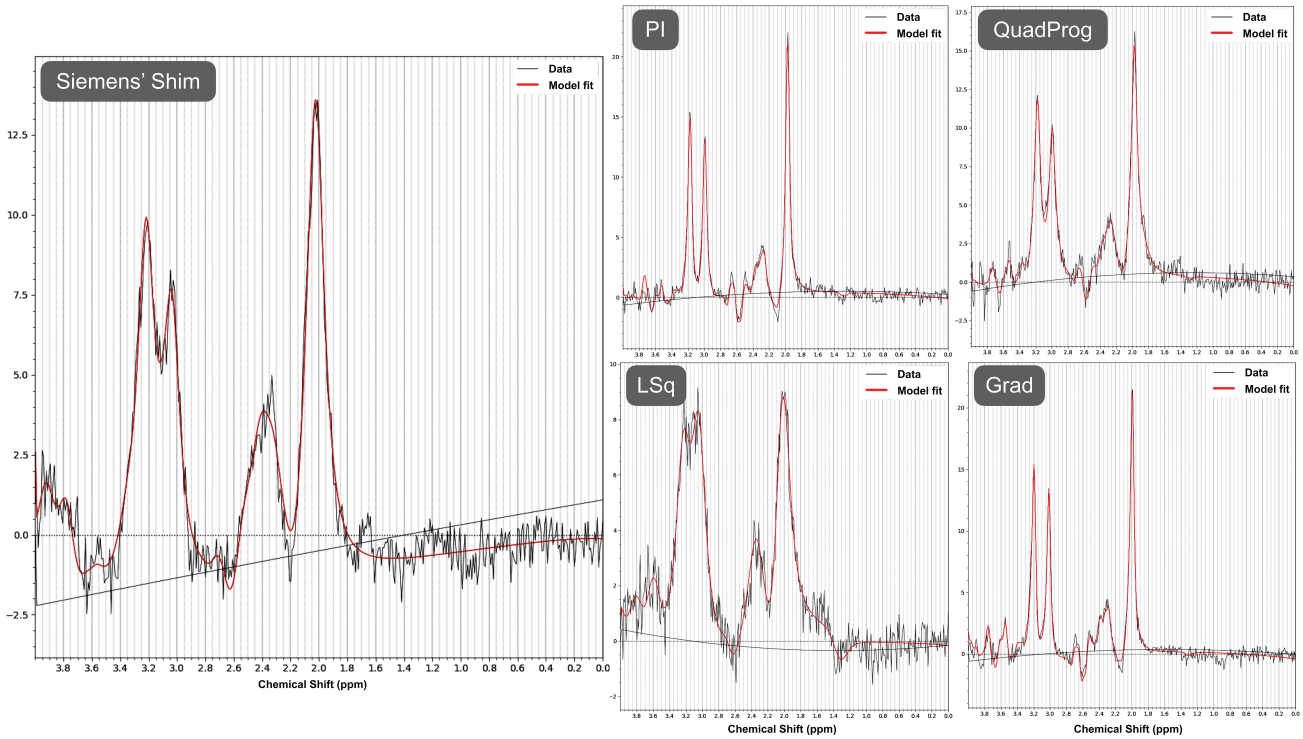

FIGURE 3 MRS spectral fit results obtained with FSL-MRS for a representative subject are shown for all five shimming algorithms.

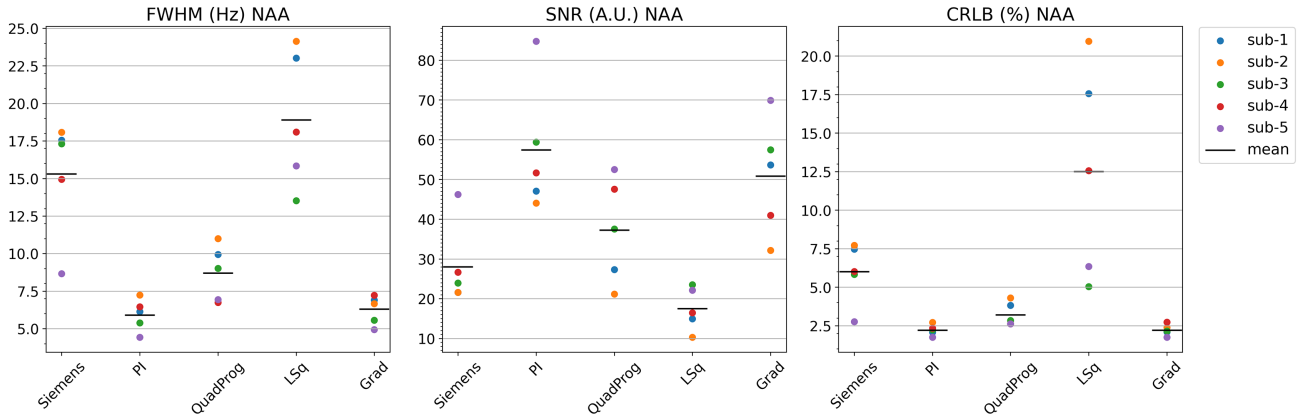

FIGURE 4 FWHM (Hz), SNR (A.U.), and percentage of CRLB for all subjects across various shim algorithms for *N*-acetylaspartate (NAA) metabolite.

for each subject. Here, we observe a consistent improvement in SNR, as well as reduced FWHM and CRLB, for the PI and Grad algorithms. Not surprisingly, among the assessed algorithms, LSq ranks the lowest in terms of SNR, FWHM, and the percentage of CRLB, largely due to the high SD of the shimmed B0 field. Following LSq, QuadProg exhibited the lowest performance, albeit much closer to the performance of the Siemens shim.

Compared to the Siemens shim, the average percent change in SNR was 105% for PI, 32% for QuadProg, −37% for LSq, and 81% for Grad method. The average percent change in the FWHM was −61% for PI, −43% for QuadProg, 23% for LSq, and −58% for Grad method. The average percent change in the CRLB was −63%, for PI, −46% for QuadProg, 108% for LSq, and −63% for Grad method.

4 | DISCUSSION

Successful MRS relies upon a well-shimmed B0 field (i.e., a B0 field with minimal inhomogeneities). In routine clinical practice, this is typically achieved using the available vendor-implemented B0 shimming tools. Various steps involved in the B0 shimming pipeline can impact the outcome of shimming, such as the accuracy of the acquired B0 map[19] or the selection of the B0 shim volume.[13] In this study, we aimed to assess how different B0 shim optimization algorithms affect single voxel MRS at 3 T.

Our results showed that, compared to Siemens' shim optimization algorithm, both the PI and Grad algorithms consistently exhibited the same level of superior performance, whereas the LSq method demonstrated inferior performance across SNR, FWHM, and CRLB metrics. The QuadProg algorithm also led to a better performance, albeit comparatively closer to the performance of the Siemens' shim. In a study by Nassirpour et al.,[14] 10 optimizers were considered for B0 shimming at 7 T, including a newly proposed algorithm called ConsTru. Only the ConsTru and vendor-provided algorithms were subsequently used to acquire MRS data at 9.4 T. Three of the 10 optimizers that were compared were similar to those used in our study, including PI, QuadProg, and LSq. Nassirpour et al. also observed that the PI method consistently achieved the best shim results. This is because PI is not an iterative algorithm but rather an analytical solution to the shim problem. In line with their study, we found that the QuadProg algorithm performed worse than the PI method. However, our results for the LSq algorithm differed from theirs. Specifically, they found that the LSq method performed better than QuadProg but worse than PI, while we found it to be the worst among the four methods we tested. By testing the numerical stability of the algorithms, we confirmed that the LSq method was the most unstable (see S2 in the supplementary information).

The use of a multi-echo sequence (such as the multi-echo approach proposed by Hetherington et al.[19]) could improve temporal accuracy, while a higher resolution B0 map could improve the spatial accuracy of our B0 maps. This may, in turn, improve the performance of different algorithms, especially given the ill-conditioned nature of the problem at hand (small shim volumes that are far from the isocenter, as is the case for MRS in the PFC will experience non-orthogonal shim fields,[30] rendering the shim problem ill-conditioned). Nevertheless, we opted to perform B0 mapping using a 3D dual-echo GRE acquisition with a protocol matching that used by Siemens for B0 shimming with their algorithm because we wanted to isolate the effects of different optimization algorithms. Given the proprietary nature of the vendor-implemented shimming algorithm, this limited our ability to use alternative B0 mapping sequences or protocols.

The ill-conditioned shimming problem that can arise in MRS is further exacerbated when dealing with higher B0 offsets within the shim volume[31] or when using a greater number of SH shim channels,[32] as is often the case at ultra-high field (7 T and higher). The study by Nassirpour et al. recommended using a regularized optimizer to address this issue. Despite the inevitable trade-off in accuracy,[14] employing such a solver becomes imperative to adhere to the system's constraints on maximum currents in ultra-high field systems. Nevertheless, our study revealed that a non-regularized bound constraint solver (Grad) performed comparably well to the analytical solution provided by the PI algorithm at 3 T. Nassirpour et al. did not mention whether the solution provided by the PI algorithm exceeded the system constraints in their study. In our case, it did not. In fact, in our study, it was the LSq algorithm that prescribed the highest currents (see S4 in the supplementary information). Nevertheless, depending on the system or shimming application, the PI may lead to prescribed shim currents that exceed the system's constraints. Therefore, we recommend the use of the Grad algorithm, which matched the performance of the PI while also considering the system's constraints.

In summary, we found that depending on the shimming algorithm, the SNR and FWHM of metabolites can improve by up to 105% and 61%, compared to what is achievable with the vendor-provided solution. This is of considerable relevance, given the clinical importance of metabolite peak-height ratios (e.g., Cho/Cr, NAA/Cr) for applications in tumor grading or dementia diagnosis.[33]

5 | CONCLUSIONS

Our work suggests that both Grad and PI algorithms significantly outperform the vendor-provided algorithm for B0 shim optimization. Specifically, they achieve a ∼66%

reduction in the SD of B0 offsets within the volume of interest and substantial improvements in MRS spectral quality metrics, including an 81% to 105% average increase in SNR, a 58% to 61% average decrease in FWHM, and a 63% average decrease in CRLB for the NAA peak. Given that the Grad algorithm matched the performance of the PI algorithm while also accommodating the system's constraints, it is better suited for B0 shimming.

ACKNOWLEDGMENTS

We thank Alexandre D'Astous for his assistance with setting up data processing pipelines within the Shimming-Toolbox, and the Functional Neuroimaging Unit for the scanning facilities, and Mathieu Guay-Paquet for providing feedback on the manuscript. The authors thank the ISMRM Reproducible Research Study Group for conducting a code review of the code (Version 4.0.0) supplied in the Data Availability Statement. The scope of the code review covered only the code's ease of download, quality of documentation, and ability to run, but did not consider scientific accuracy or code efficiency.

FUNDING INFORMATION

This research was undertaken thanks, in part, to funding from the Canada First Research Excellence Fund (TransMedTech Institute), the Natural Sciences and Engineering Research Council of Canada, and Polytechnique Montreal.

DATA AVAILABILITY STATEMENT

Data: https://osf.io/s3gwv/. Code: https://github.com/neuropoly/single_voxel_mrs_b0_shimming/releases/tag/v4.0.0.

ORCID

Behrouz Vejdani Afkham https://orcid.org/0000-0003-3923-5117
Eva Alonso-Ortiz https://orcid.org/0000-0001-6590-7234

REFERENCES

1. Koch KM, McIntyre S, Nixon TW, Rothman DL, de Graaf RA. Dynamic shim updating on the human brain. *J Magn Reson*. 2006;180:286-296.
2. Juchem C, De Graaf RA. B0 magnetic field homogeneity and shimming for in vivo magnetic resonance spectroscopy. *Anal Biochem*. 2017;529:17-29.
3. Tkác I, Andersen P, Adriany G, Merkle H, Ugurbil K, Gruetter R. In vivo 1H NMR spectroscopy of the human brain at 7 T. *Magn Reson Med*. 2001;46:451-456.
4. Haase A, Frahm J, Hänicke W, Matthaei D. 1H NMR chemical shift selective (CHESS) imaging. *Phys Med Biol*. 1985;30:341-344.
5. Schenck JF. The role of magnetic susceptibility in magnetic resonance imaging: MRI magnetic compatibility of the first and second kinds. *Med Phys*. 1996;23:815-850.
6. Lin A, Tran T, Bluml S, Merugumala S, Liao H-J, Ross B. Guidelines for acquiring and reporting clinical Neurospectroscopy. *Semin Neurol*. 2013;32:432-453.
7. Durand E, van de Moortele P-F, Pachot-Clouard M, Le Bihan D. Artifact due to B0 fluctuations in fMRI: correction using the k-space central line. *Magn Reson Med*. 2001;46:198-201.
8. Xu N, Fitzpatrick JM. Dynamic field mapping and distortion correction for fMRI. In: *Medical Imaging: Image Processing*. (Vol. 6512). SPIE; 2007:65121M. doi:10.1117/12.709509
9. Juchem C, Nixon TW, McIntyre S, Boer VO, Rothman DL, de Graaf RA. Dynamic multi-coil shimming of the human brain at 7T. *J Magn Reson*. 2011;212:280-288.
10. Liao HV, Coello EJU, Lin AP. Performance of automatic B0 shim modes for brain MR spectroscopy on 7T and 3T. *Proceedings of the 28th Annual Meeting of ISMRM [Virtual]*. Vol 28. International Society for Magnetic Resonance in Medicine; 2020:S31.
11. Deelchand DK, Kantarci K, Öz G. Improved localization, spectral quality, and repeatability with advanced MRS methodology in the clinical setting. *Magn Reson Med*. 2018;79:1241-1250.
12. Zhong X, Lyubich YM, DeVito T, Shah S, Knight-Scott J. Improving in vivo 1H-MRS with robust automated shim techniques: a comparison study of FASTESTMAP and GRESHIM. In *Proceedings of the 20th scientific meeting, International Society for Magnetic Resonance in Medicine*. Vol 4397. ISMRM; 2012.
13. Pan JW, Terpstra MJ, Moon C-H, Hetherington HP. Map-based B0 shimming for single voxel brain spectroscopy at 7T. *NMR Biomed*. 2023;36:e5021.
14. Nassirpour S, Chang P, Fillmer A, Henning A. A comparison of optimization algorithms for localized in vivo B0 shimming. *Magn Reson Med*. 2018;79:1145-1156.
15. Gruetter R, Boesch C. (1992) fast, noniterative shimming of spatially localized signals. *In vivo* analysis of the magnetic field along axes. *J Magn Reson*. 1969;96:323-334.
16. Gruetter R. Automatic, localizedin vivo adjustment of all first-and second-order shim coils. *Magn Reson Med*. 1993;29:804-811.
17. Shen J, Rycyna RE, Rothman DL. Improvements on an in vivo automatic shimming method (FASTERMAP). *Magn Reson Med*. 1997;38:834-839.
18. Gruetter R, Tkáč I. Field mapping without reference scan using asymmetric echo-planar techniques. *Magn Reson Med*. 2000;43:319-323.
19. Hetherington HP, Chu W-J, Gonen O, Pan JW. Robust fully automated shimming of the human brain for high-field 1H spectroscopic imaging. *Magn Reson Med*. 2006;56:26-33.
20. Chang P, Nassirpour S, Henning A. Modeling real shim fields for very high degree (and order) B0 shimming of the human brain at 9.4 T. *Magn Reson Med*. 2018;79:529-540.
21. D'Astous A, Cereza G, Papp D, et al. Shimming toolbox: an open-source software toolbox for B0 and B1 shimming in MRI. *Magn Reson Med*. 2023;89:1401-1417.
22. Goldfarb D, Idnani A. A numerically stable dual method for solving strictly convex quadratic programs. *Math Program*. 1983;27:1-33.
23. Zhu C, Byrd RH, Lu P, Nocedal J. Algorithm 778: L-BFGS-B: Fortran subroutines for large-scale bound-constrained optimization. *ACM Trans Math Softw*. 1997;23:550-560.
24. Keskar N, Wächter A. A limited-memory quasi-Newton algorithm for bound-constrained non-smooth optimization. *Optim Methods Softw*. 2019;34:150-171.

25. Barrow D, Kourentzes N, Sandberg R, Niklewski J. Automatic robust estimation for exponential smoothing: perspectives from statistics and machine learning. *Expert Syst Appl*. 2020;160:113637. doi:10.1016/j.eswa.2020.113637
26. Clarke WT, Stagg CJ, Jbabdi S. FSL-MRS: an end-to-end spectroscopy analysis package. *Magn Reson Med*. 2021;85:2950-2964.
27. Hui SCN, Saleh MG, Zöllner HJ, et al. MRSCloud: a cloud-based MRS tool for basis set simulation. *Magn Reson Med*. 2022;88:1994-2004.
28. Landheer K, Juchem C. Are Cramér-Rao lower bounds an accurate estimate for standard deviations in in vivo magnetic resonance spectroscopy? *NMR Biomed*. 2021;34:e4521.
29. Wilson M, Andronesi O, Barker PB, et al. Methodological consensus on clinical proton MRS of the brain: review and recommendations. *Magn Reson Med*. 2019;82:527-550.
30. Hoult DI. "Shimming" on spatially localized signals. *J Magn Reson* 1969. 1987;73:174-177.
31. Kim D-H, Adalsteinsson E, Glover GH, Spielman DM. Regularized higher-order in vivo shimming. *Magn Reson Med*. 2002;48:715-722.
32. Fillmer A, Kirchner T, Cameron D, Henning A. Constrained image-based B0 shimming accounting for "local minimum traps" in the optimization and field inhomogeneities outside the region of interest. *Magn Reson Med*. 2015;73:1370-1380.
33. Lin A, Ross BD, Harris K, Wong W. Efficacy of proton magnetic resonance spectroscopy in neurological diagnosis and neurotherapeutic decision making. *NeuroRx*. 2005;2:197-214.

SUPPORTING INFORMATION

Additional supporting information may be found in the online version of the article at the publisher's website.

Figure S1: The distribution of B0 offsets across the whole-brain for B0 maps acquired before shimming by each algorithm is shown for one subject (marked as "Unshimmed"). The simulated shimmed B0 maps (marked as "Shimmed") are also presented. The standard deviation (SD) is noted beside each violin plot. There was no significant difference between the shimmed maps of the different algorithms for whole-brain shimming ($p < 0.01$).

Figure S2: Results of the numerical stability test: By adding Gaussian-distributed random noise (with the maximum noise amplitude being 1% of the fieldmap) to the pre-shimming B0 maps of 3 subjects, we generated a total of 150 noisy fieldmaps (50 per subject). Each algorithm was then used to shim these 150 fieldmaps. The plot shows the distribution of all 150 shimmed B0 maps (simulated) for each algorithm using the noisy input fieldmaps. The standard deviation (SD) for each algorithm is shown on the plot.

Figure S3: MRS spectral fit results obtained with FSL-MRS for all five subjects and each shimming algorithm.

Figure S4: The plot illustrates the current calculated by each optimizer for each shim coil. The unit of current is in μT/m for the first-order shim terms and μT/m^2 for the second-order terms. The data includes all five subjects of the study, with the solid line indicating the average current for each optimizer across subjects. Additionally, the plot shows the system's limits for the maximum and minimum current per coil.

How to cite this article: Vejdani Afkham B, Alonso-Ortiz E. On the impact of B0 shimming algorithms on single-voxel MR spectroscopy. *Magn Reson Med*. 2024;1-9. doi: 10.1002/mrm.30257